

RESEARCH LETTER

10.1002/2017GL076644

GIA Model Statistics for GRACE Hydrology, Cryosphere, and Ocean Science

L. Caron¹, E. R. Ivins¹, E. Larour¹, S. Adhikari¹, J. Nilsson¹, and G. Blewitt^{2,3}

¹Jet Propulsion Laboratory, California Institute of Technology, Pasadena, CA, USA, ²Nevada Bureau of Mines and Geology, University of Nevada, Reno, Reno, NV, USA, ³Department of Physics, University of Nevada, Reno, Reno, NV, USA

Key Points:

- We perform an inversion of GIA based on GPS and RSL data, varying mantle rheology and ice history
- We derive formal uncertainty calculation of present-day GIA, reflecting 128,000 forward models
- The uncertainty is larger than previously reported and than GRACE RL05 inherent uncertainty estimation

Supporting Information:

- Supporting Information S1

Correspondence to:

L. Caron,
lambert.caron@jpl.nasa.gov

Citation:

Caron, L., Ivins, E. R., Larour, E., Adhikari, S., Nilsson, J., & Blewitt, G. (2018). GIA model statistics for GRACE hydrology, cryosphere, and ocean science. *Geophysical Research Letters*, 45, 2203–2212. <https://doi.org/10.1002/2017GL076644>

Received 4 DEC 2017

Accepted 19 JAN 2018

Published online 6 MAR 2018

Abstract We provide a new analysis of glacial isostatic adjustment (GIA) with the goal of assembling the model uncertainty statistics required for rigorously extracting trends in surface mass from the Gravity Recovery and Climate Experiment (GRACE) mission. Such statistics are essential for deciphering sea level, ocean mass, and hydrological changes because the latter signals can be relatively small (≤ 2 mm/yr water height equivalent) over very large regions, such as major ocean basins and watersheds. With abundant new >7 year continuous measurements of vertical land motion (VLM) reported by Global Positioning System stations on bedrock and new relative sea level records, our new statistical evaluation of GIA uncertainties incorporates Bayesian methodologies. A unique aspect of the method is that both the ice history and 1-D Earth structure vary through a total of 128,000 forward models. We find that best fit models poorly capture the statistical inferences needed to correctly invert for lower mantle viscosity and that GIA uncertainty exceeds the uncertainty ascribed to trends from 14 years of GRACE data in polar regions.

1. Introduction

As society now faces the long-term consequences of a warming climate, a primary goal of space gravimetry is to determine trends in surface water transport: in the cryosphere, oceans, and in land hydrology. The Gravity Recovery and Climate Experiment (GRACE) satellite mission has three official data processing centers (Center for Space Research (CSR), University of Texas; Jet Propulsion Laboratory (JPL), Pasadena; and GeoForschungZentrum, Potsdam) that produce monthly Stokes coefficients (Wouters et al., 2014), from which gravity changes can be reconstructed over 2002–2017. While one of the great challenges to GRACE scientists is to minimize the impact of various sources of uncertainty (e.g., Chen, Wilson, et al., 2017; Eicker et al., 2016; Wiese et al., 2016), there is an agreement that after spatial and temporal filtering is applied (e.g., Save et al., 2012; Swenson & Wahr, 2006), the uncertainty level for inferring mass changes is ~ 1 cm/yr water height equivalent over spatial scales of 300–450 km, though this estimate is highly dependent upon the target geometry and submonthly time dependence (e.g., Velicogna & Wahr, 2013). Only through very rigorous treatment and propagation of uncertainties can a reliable trend in GRACE data be retrieved below the 5 mm/yr level at watershed scales (Schumacher et al., 2016). This is essential for determining secular change in the water cycle (e.g., Eicker et al., 2016; Famiglietti & Rodell, 2013). In large ocean basins, GRACE trends are more accurate, generally by an order of magnitude (Johnson & Chambers, 2013; Quinn & Ponte, 2010). These accuracies impact our ability to improve closure of global water budget (Reager et al., 2016; Rietbroek et al., 2016) and to both quantify and disambiguate the sources of heat and mass change in the global oceans (Chen, Zhang, et al., 2017; Llovel et al., 2014). The recovery of surface mass trends from GRACE requires a background glacial isostatic adjustment (GIA) model.

GIA models compute the solid Earth viscoelastic response to forcing applied by surface mass redistributions during waxing and waning of Pleistocene glaciations. A host of improvements in global GIA models have evolved over the past decades. New models (including the ICE-6G model, Peltier et al., 2015; Purcell et al., 2016; Roy & Peltier, 2017, and the latest version of the Australian National University (ANU) model, Lambeck et al., 2014, 2017) use considerably more data that constrain moraine position and dating during the ice sheet collapse phase (e.g., Gowan et al., 2016; Simon et al., 2017; Tarasov et al., 2012). Space geodesy has a growing role (Milne et al., 2001), along with an ever greater volume of relative sea level (RSL) data (Murray-Wallace & Woodroffe, 2014). Combined Global Positioning System (GPS) and space gravimetry now impact current

©2018. The Authors.

This is an open access article under the terms of the Creative Commons Attribution-NonCommercial-NoDerivs License, which permits use and distribution in any medium, provided the original work is properly cited, the use is non-commercial and no modifications or adaptations are made.

model constraint paradigms (Bevis et al., 2012; Blewitt et al., 2016; Ivins et al., 2013; Khan et al., 2016; Tamisiea et al., 2007). The advancements have led modelers to consider ever more sophisticated approaches to assimilating data (e.g., Caron et al., 2017; Martinec et al., 2014). We propose such an advancement here using Bayesian framework with a wealth of new GPS time series from 459 sites and 11,451 RSL data.

The approach to treating uncertainties in GIA models has generally been to employ a limited number of models (≤ 100), often with similar model parameters. GIA uncertainties are especially troublesome in ice covered areas, and specialized treatments of GIA have been generated for Alaska, Canadian Arctic, Greenland by Sasgen et al. (2012). Antarctica is especially problematic, as the gravimetrically recorded secular change signature and GIA have similar size and geometry (Ivins et al., 2011; King et al., 2012; Shepherd et al., 2012). However, none of these specialized models are global in nature and therefore fail to predict the secular variations of the low-degree geoid, nor do they leverage advantage from the expanding global RSL data sets. The low order field aids our understanding of bulge migration (Sella et al., 2007), rotational feedback (Mitrovica et al., 2015), geocenter motion, and changes detected by satellite laser ranging (SLR) (e.g., Bonin et al., 2018; Eanes & Bettadpur, 1996; Sośnica et al., 2015). GIA uncertainty on ocean mass and sea level trends have been treated by Tamisiea (2011), and the influence of forebulge collapse on North American hydrology has been discussed by Roy and Peltier (2017). However, such studies rely on comparison in prediction spreads rather than on rigorously derived uncertainties. Here we provide trends with formal uncertainty estimation that can be employed in multidisciplinary studies emerging from GRACE, SLR, and other geodetic data sets.

2. Method

2.1. Constraining Data Set and Forward Modeling

We solve the classical loading equations for a compressible Maxwell solid Earth and a surface loading driven by the buildup and collapse of ice sheets during the last 122 kyr (e.g., Vermeersen et al., 1996). Our calculations are performed using spherical harmonic truncated at degree 89 (1° spatial resolution) in the center of mass frame. Included are feedbacks from Earth rotation (Milne & Mitrovica, 1998) and coastlines that migrate in accordance with mass change and solution of the sea level equation (e.g., Lambeck et al., 2003). Although the method follows Caron et al. (2017), several new features are introduced that are both fundamental and significant. We expand the compilation of RSL constraints by 5,371 new records, bringing the total to 11,451 (see Figure 1), now incorporating minimum and maximum RSL bounds over North America from Dyke et al. (2002) and local mean sea level from Milne et al. (2005) in South America and Briggs and Tarasov (2013) and Verleyen et al. (2017) in Antarctica.

VLM trends determined by 459 GPS stations distributed in Europe, North America, and Antarctica are also incorporated here. The data are processed using the JPL's GIPSY OASIS II software and the GPS raw RINEX files that are provided by the UNAVCO and International GNSS Service data centers. The time series are generated via the method described by Blewitt et al. (2016) and available on the Nevada Geodetic Laboratory web portal. We culled these time series, noting that the pertinent data are generally located within 2,500 km of the former Last Glacial Maximum (LGM) ice domes. Especially important is avoidance of sites south of 34°N in North America, wherein non-GIA processes can easily manifest ~ 1 mm/yr signatures (Jones et al., 2016; Kuchar et al., 2017). Time series were required to be longer than 3.4 years, exhibit a signal-to-noise ratio of at least 3, and did not include stations susceptible to any known sources of corrupting tectonic or anthropogenic signal. A few exceptions were made by including time series as short as 2.4 years but located in places where measured GIA uplift rates were ≥ 10 mm/yr and of signal-to-noise ratio above 10. To correct Antarctic sites from elastic rebound caused by present-day ice mass change, we employ CryoSat-2 altimetry surface elevation change estimates following the processing of Nilsson et al. (2016), with several modifications; rates of elevation change are solved for on a 500 m grid, similar to McMillan et al. (2014), and interpolated to 1 km using inverse distance interpolation to fill empty grid nodes. The estimated rates are also corrected for changes in scattering regime, using the waveform parameters described in Flament and Rémy (2012). Finally, we use the method of Adhikari et al. (2016) to compute the high-resolution elastic response assuming the load density to be between 450 and 917 kg m^{-3} .

A scaled version of the ANU ice history (Lambeck et al., 2010, 2014) was employed, except for Antarctica and Patagonia where ice models having more contemporary constraints are available (Briggs & Tarasov, 2013; Ivins & James, 2004; Ivins et al., 2013; Whitehouse, Bentley, Milne, et al., 2012). Improving the Southern Hemisphere model over that used by Caron et al. (2017) is key to developing improved global constraints on the parameters and to reduce trade-offs between ice history and mantle viscosity. The ice regions allow separate

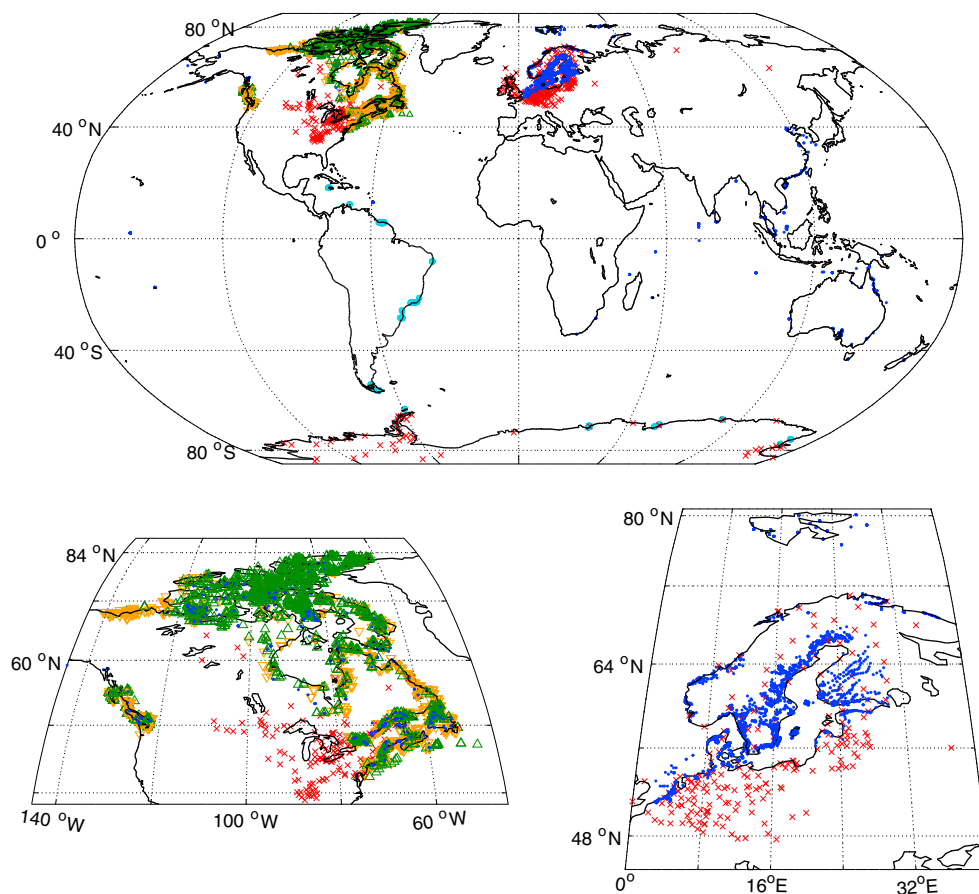


Figure 1. Data distribution used for glacial isostatic adjustment inversion constraint. Blue circles: mean local relative sea level (RSL) from the compilation used in Caron et al. (2017); orange and green triangles: RSL maximum and minimum bounds, respectively, from Dyke et al. (2002); teal circles: mean local RSL from the compilations of Briggs and Tarasov (2013), Milne et al. (2005), and Verleyen et al. (2017); and red crosses: Global Positioning System trends from Blewitt et al. (2016).

load adjustment parameters to apply for Laurentide and Cordilleran ice sheets (see supporting information Figure S1). Mountain glaciers area also included from the ANU model (Lambeck et al., 2010, 2014).

2.2. Cost Function and Bayesian Probability

To address the heterogeneity in our set of constraints, our analysis applies weighting, respecting three aspects of the data: its reported formal uncertainty, inherent redundancy of information content, and the necessity for creating a balance among RSL and GPS data sets.

As is classically done, we translate formal uncertainty into inversely proportional weights.

To suppress the effects of redundant information, we generate an ensemble of model predictions at the space and time coordinates of each data point from a random and uniform exploration of the parameter space, without consideration of the residuals. We assume that if two data sites reveal any correlation of their model predictions, despite blind variation of the parameters, they contain partially redundant information. This may occur, for example, when data points have similar coordinates. A weight for this redundancy is expressed as follows:

$$w_i = \frac{K}{\sum_{j=1}^{N_{\text{data}}} \rho_{ij}}, \quad (1)$$

where $\rho_{i,j}$ is the Pearson correlation coefficient between the ensembles of predictions at sites i and j , N_{data} the total number of data, and K a normalization constant so that $\sum_i \frac{w_i}{N_{\text{data}}} = 1$.

Both GPS and RSL data sets are treated as having equal importance in our inversion, despite the number of data in each set being vastly different. An additional layer of weighting is thus applied such that each data set a priori accounts for 50% of the misfit:

$$N_{\text{RSL}} \times w_{\text{RSL}}^2 = N_{\text{GPS}} \times w_{\text{GPS}}^2 = (N_{\text{RSL}} + N_{\text{GPS}})/2, \quad (2)$$

where N_{RSL} and N_{GPS} are the number of RSL and GPS data points and w_{RSL} and w_{GPS} weights attributed to RSL and GPS data points, respectively.

For a given forward model and data point i , our misfit function is expressed as follows:

$$J_i = \begin{cases} 0, & \text{if } y_{\text{model},i} - y_{\text{data},i} > 0 \text{ and data point } i \text{ is a RSL minimum bound,} \\ 0, & \text{if } y_{\text{model},i} - y_{\text{data},i} < 0 \text{ and data point } i \text{ is a RSL maximum bound,} \\ \frac{(y_{\text{model},i} - y_{\text{data},i})w_d}{\sigma_i}, & \text{otherwise,} \end{cases} \quad (3)$$

where w_d indicates either w_{GPS} or w_{RSL} , depending on data i , y_{model} the model predictions, y_{data} the constraining data set, and σ the associated uncertainty. This allows us to compute the likelihood probability density function (PDF), assuming a uniform prior:

$$p = \exp\left(-\frac{1}{2N_{\text{data}}} \sum_{i=1}^{N_{\text{data}}} J_i^2\right). \quad (4)$$

This probability represents how likely a given model is to explain our constraining data set and serves as a weighting factor in our statistics of GIA parameters and signal. A simulated annealing algorithm samples the PDF in the space formed by both the Earth structure and ice history parameters.

3. Results and Discussion

3.1. Character of the GIA PDF

Figure 2 shows the PDF derived from our model ensemble and projected against every pair of parameters varied in the inversion (see supporting information Figures S7 and S8 for the role of RSL and GPS data sets, respectively). Caron et al. (2017) previously found a notable trade-off of lower mantle viscosity with the coefficient scaling the Antarctic ice sheet, leading the latter to accommodate the mass budget requirements derived from the far-field RSL record (Briggs & Tarasov, 2013; Ivins et al., 2013; Whitehouse, Bentley, & Le Brocq, 2012), especially at LGM (Hanebuth et al., 2009). This trade-off is now substantially reduced, owing to the inclusion of direct constraint data in Antarctica. Note the breadth of the red region in Figure 2: a large range of models exhibits a likelihood comparable with the best fitting model (white circle). However, the latter is a quite poor indicator of this range of models. For example, the “best fit” lower mantle viscosity is more akin to an end-member solution, rather far from an average (white cross). This illustrates the potential danger in using single best fit models for formulating GIA corrections (e.g., Karegar et al., 2017), especially without associated uncertainty (also see Geruo et al., 2013; Paulson et al., 2007; Peltier, 2004). This systematic underestimation of the lower mantle viscosity is responsible for an enhanced degree 2, 1 pattern associated with rotational feedback (see supporting information Figure S2). Here we argue that robust statistical characterization of GIA must elucidate properties of the entire distribution of models, and hence, the use of expected values is more meaningful than best fitting values. The former are accompanied by robust uncertainty quantification (see supporting information Table S1) by using the statistics derived from our model ensemble.

3.2. Bayesian Prediction

Analogous insights are revealed in Bayesian GIA predictions. Figure 3 shows the expectation and standard deviation of the present-day gravity rate due to GIA corresponding to our PDF. Supporting information Figures S3 and S4 give the predictions and uncertainties of uplift and geoid rates, respectively. Note that our measure of uncertainty is larger in the near field (areas close to the deglaciation centers) than in the far field due to larger amplitude of the signal. Uncertainty peaks at a similar value for all ice sheets, despite the expectation being larger around larger ice sheets. This simple balance is a property of the scaling process, wherein a small variation of the larger ice sheets results in a similar amount of misfit to a larger percentage change in the smaller model ice sheets. Improving local constraints from the data set and increasing the number of scaling factors would obviously influence this pattern as well. Note that we employ few data for constraining the Greenland and Cordilleran ice sheets.

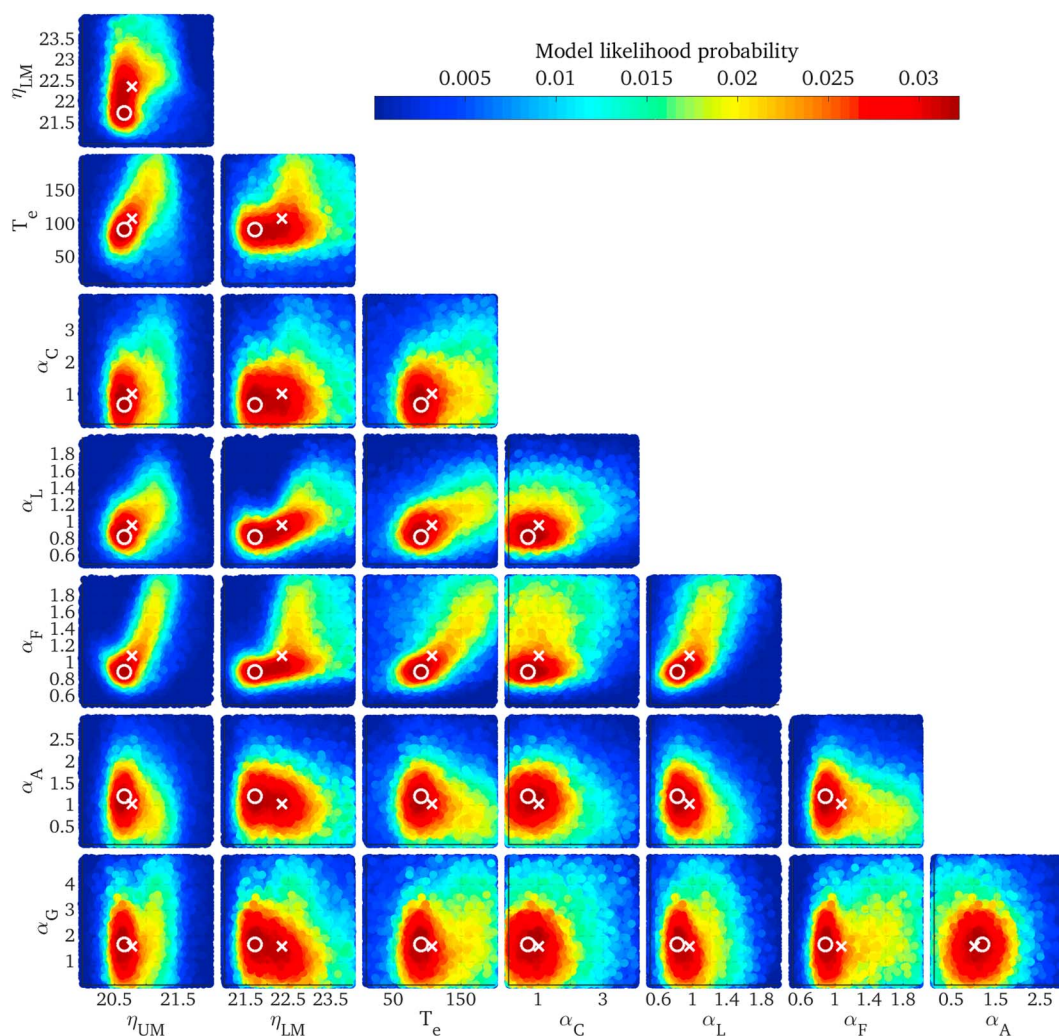


Figure 2. Likelihood probability distribution projected in 2-D spaces formed by each pair of parameters. η_{UM} : upper mantle viscosity (\log_{10} (Pa s)), η_{LM} : lower mantle viscosity (\log_{10} (Pa s)), T_e : elastic lithosphere thickness (km), α_C , α_L , α_F , α_A , and α_G : regional ice scaling coefficients for the Cordilleran, Laurentide, Fennoscandian, Antarctic, and Greenland ice sheets, respectively. Note that models with larger probability are plotted on top of lower probability models. The white circle and white cross indicate the best fitting and expected values, respectively.

The lack of the aforementioned balance in the relative uncertainty measure has significant consequences. It has local minima at the deglaciation centers, being as small as $\sim 12.3\%$ of the gravity rate expectation, and then grows very large as the expectation tends to 0. We find its spatial median value to be $\sim 43.7\%$, much larger than the 20% recently reported by, for example, Karegar et al. (2017). The reason for this largely owes to the contribution from oceanic regions, where the GIA signal is both small and poorly constrained, which highlights the importance of considering uncertainties at the global scale when dealing with GIA corrections. This is especially true for analyzing secular ocean mass trends in the intermediate and far field where GRACE can, in theory, be a powerful tool for direct measurement of mass-related gravity changes (Cazenave & Cozannet, 2014; Chambers & Schröter, 2011; Hsu & Velicogna, 2017). GIA produces large gravity changes in the environs surrounding the Arctic Ocean, where GRACE has been used to decipher mass loss due to regional freshening (Morison et al., 2007). Here GIA uncertainty is an extremely relevant issue and here-to-for has been treated only with the best fit approaches.

3.3. Uncertainty Versus Bias

For our purpose, it is important to describe how the Bayesian GIA uncertainty can be compared to intrinsic biases that arise in the sets of Stokes coefficients delivered in official GRACE releases. These coefficients have provided unique information about interannual, seasonal, and interseasonal surface mass transport

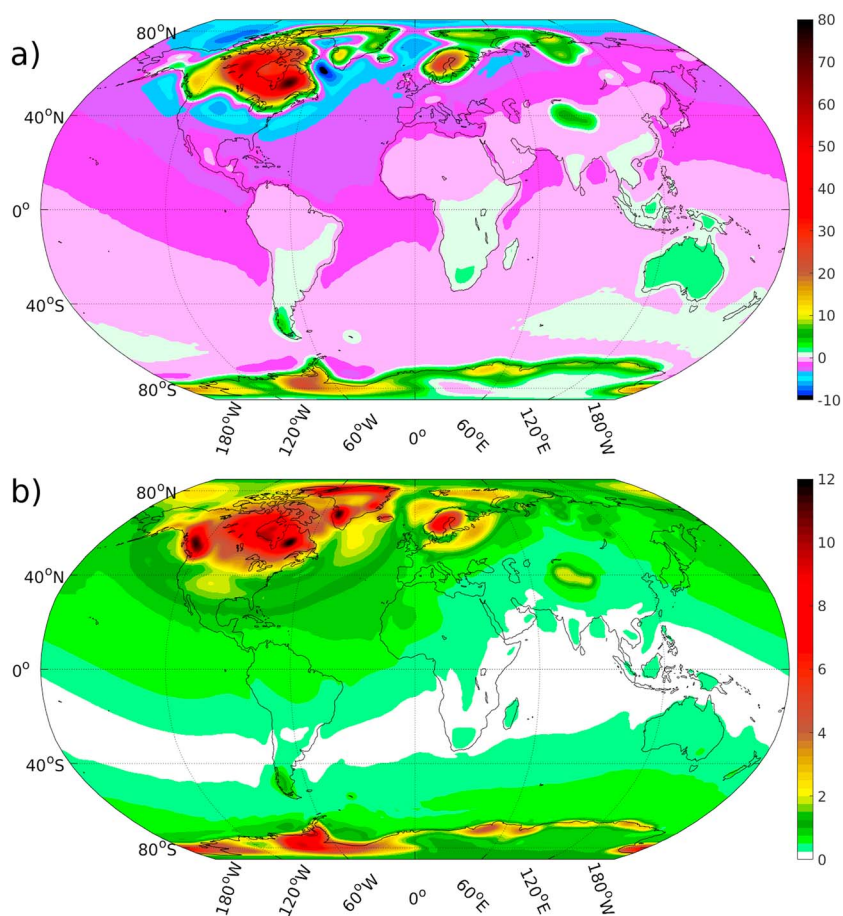


Figure 3. Maps of expectation (a) and standard deviation (b) of present-day gravity trend, based on the probability density function, in millimeter per year water height equivalent. Note that the color scale is nonlinear.

(Wahr et al., 1998). The released fields are burdened by a layered complexity, and it is difficult to fully track uncertainties. Many are inherent to ranging and other required measurements (including GPS clock uncertainty) and to imperfections of the background dealiasing fields. Generally, the level of uncertainty to apply when using GRACE is difficult to quantify (see Velicogna & Wahr, 2013), and the full covariance matrix for each of the spherical harmonic coefficients is needed (Wu et al., 2010). Advanced mascon methods show promise for providing fields of reduced uncertainty (Save et al., 2016; Watkins et al., 2015). In Figure 4, we show a polar perspective comparison, motivated by the importance of GIA models for decontaminating GRACE trends of GIA-related mass change when determining the ice sheet contribution to sea level rise (Ivins et al., 2013; Martín-Español et al., 2016; Sasgen et al., 2012; Shepherd et al., 2012) or to changes in the polar oceans (Morison et al., 2007; Ponte & Piecuch, 2014). Note how GIA uncertainty clearly exceeds the discrepancy between CSR and JPL GRACE solutions, especially in Greenland, the Canadian Arctic, and West Antarctica. As future space gravimetry will improve accuracy and ameliorate many of the problems with correlated errors, it will be essential to improve GIA models and to properly characterize their uncertainty.

3.4. Caveats

There are limitations in our approach. For example, we do not account for lateral heterogeneity in viscosity, as our 1-D Earth structure model represents some azimuthal average. This fact creates a bias that retrieves structure more appropriate to cratonic mantle, where most of the signal is generated and measured (Caron et al., 2017; Nordman et al., 2015). This is problematic when regional viscosity is significantly different, and there has been robust Neoglacial or Little Ice Age mass transfer (e.g., Richter et al., 2016). For example, near the coast of Marie Byrd Land where the upper mantle viscosity is thought to be very low, possibly near 10^{18} Pa s, our ensemble predicts 1.96 ± 0.65 , 1.33 ± 0.49 , and 1.64 ± 0.60 mm/yr of uplift, while the observed values are 12.1 ± 2.22 , 22.6 ± 2.71 , and 37.0 ± 5.5 mm/yr, respectively. Deformation is relaxing much faster

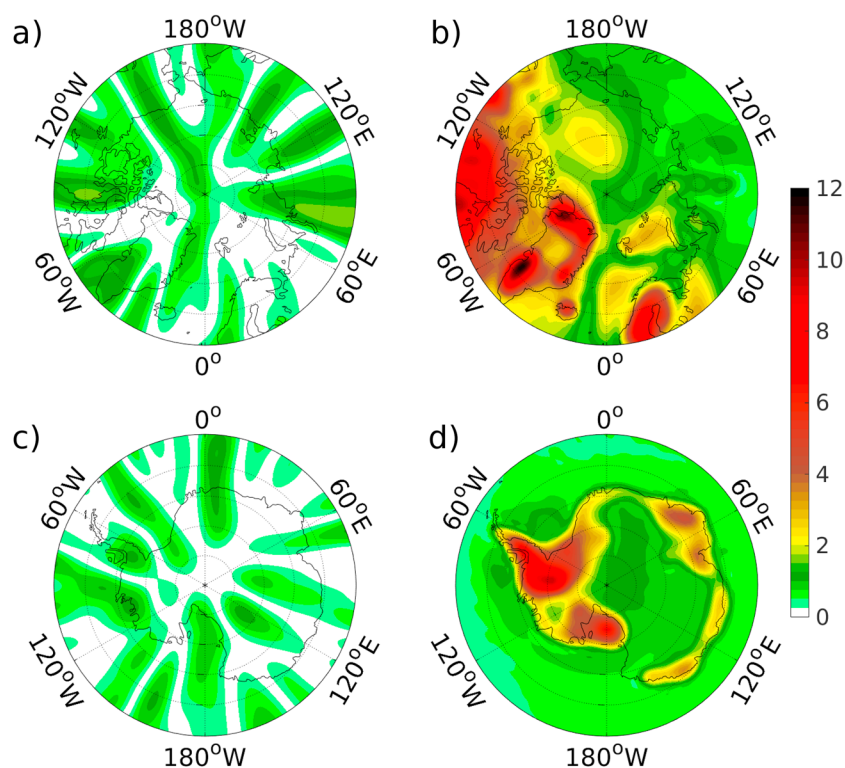


Figure 4. Absolute differences (millimeter per year water height equivalent) between Center for Space Research and Jet Propulsion Laboratory Release 05-based trend solutions (a and c) and uncertainty for Bayesian glacial isostatic adjustment reconstruction (b and d) in polar regions north and south of 60° latitude. Figures 4a and 4c use a Gaussian filter radius of 450 km (Jekeli, 1981). Gravity Recovery and Climate Experiment trends were determined using coefficient releases from April 2002 to March 2016 and \hat{C}_{20} replacement.

with low viscosity, and the prediction of both response amplitude and model load history would, therefore, be poorly tuned to regional decay times operating in the real Earth. Our residuals (supporting information Figure S5) suggest cautionary application to West Antarctica and the Antarctic Peninsula. Dedicated regional models that include 3-D viscosity structure (Kaufmann et al., 2005; Sasgen et al., 2017; van der Wal et al., 2015), although not yet accounting for formal uncertainty, may be better suited for these regions.

Other limitations include the fact that we cannot account for every possible ice sheet position and timing scenario. Our discretization of the ice history assumes no more than six coefficients, each lacking time dependence. This means that we are saddled to certain biases in the nominal ice history model that we scale, thus underestimating the uncertainty in the PDF. Indeed, comparisons with the ICE-6G/VM5a (Purcell et al., 2016, see supporting information Figure S2) model predictions suggest statistically irreconcilable discrepancy. New constraints on dates and sizes of past ice complexes continue to emerge, and especially promising are Arctic Russia, Siberia, and Canada for providing new RSL and VLM data. New evidence has recently reinvigorated the idea that northeasternmost Eurasia may have been more extensively glaciated at LGM than recent models allow for (Cronin et al., 2017). Such ice complexes should be considered as forward model features of our algorithms in the future.

4. Conclusion

An ensemble of 128,000 forward model runs is informed by a data set of 11,451 RSL and 459 GPS data, jointly varying both the Earth rheological structure and ice history. Through Bayesian statistics, we characterize the present-day GIA signal and find the following:

1. Most GIA correction for GRACE have focused on providing a best fitting model and ranges based on differentiating a small set of models, which lead to underestimating the lower mantle viscosity and biases in some long-wavelength characteristics (e.g., forebulge extent). In contrast, the use of Bayesian statistics provides better representation of the distribution of likely GIA models and their parameters.

2. We provide formal estimations of the expectation and uncertainty of present-day GIA signal, which can be used as corrections to geophysical interpretations of present-day geodetic measurements and, in particular, those for GRACE gravimetry.
3. The uncertainty here is generally greater than in past scientific reports. We find the global median of relative uncertainty to be about 44% of the gravity rate. We may still be somewhat underestimating this uncertainty due to limitations in our treatment of ice history and azimuthally averaged rheology.
4. In regions above 60° latitude, our uncertainty in gravity trends clearly exceeds the discrepancy between CSR and JPL GRACE Release 05.

Further progress to obtain realistic GIA uncertainties can be made by improving the available constraints. For Greenland, there are additional GPS and RSL data sets that can be used to reduce our estimates of uncertainties in a future analysis. Future work should also more closely scrutinize lateral variations of the viscosity and associated local ice history, particularly in Antarctica and Greenland.

The results presented in this paper are extremely important for improving long-wavelength error statistics. Comparing our results with Stokes coefficient rates derived from SLR (Cheng et al., 2011) (see supporting information Table S2), we can see that 1σ for GIA modeled \dot{C}_{20} is a full 50% of the SLR retrieved value, which is commonly used as a replacement for GRACE analysis (Chen, Wilson, et al., 2017; Watkins et al., 2015; Wouters et al., 2014). In other cases, the GIA 1σ value is close to the SLR-determined rate. It is critical that these statistics be properly folded into analyses of ice mass balance for the space gravimetry observing period extending back to 1992 such as recently treated by Sošnica et al. (2015) and Bonin et al. (2018).

Many VLM features recovered from the Bayesian model are tantalizingly robust and will be reported in a follow-on paper. The features shown in supporting information Figure S3 include subsidence of -1 to -1.5 mm/yr in the southwesternmost United States and the -2.0 ± 0.4 mm/yr peak subsidence in the Gulf of Mexico, regions lacking GPS model constraint, as these are susceptible to a myriad of other geophysical origins.

Acknowledgments

This research was carried out at the Jet Propulsion Laboratory (JPL), California Institute of Technology, under a contract with the National Aeronautics and Space Administration (NASA). We thank the following sponsors: the NASA Postdoctoral Program and ROSES funds for the GRACE Science Team (grant 967701.02.03.01.81), Cryosphere Program (grant 967701.02.03.01.30), NASA Sea-level Change Team (grant 509496.02.08.10.65), and Earth Surface and Interior Focus Areas (grant 281945.02.47.03.86). Spherical harmonic computations were performed using SHTOOLS (Wieczorek et al., 2016) for Bayesian models and software of Holmes and Featherstone (2002) for GRACE analysis. We thank Kurt Lambeck and Anthony Purcell for providing the ANU model and part of our RSL compilation. We thank two anonymous reviewers for their constructive comments and suggestions. Statistics on present-day uplift, geoid, gravity and Stokes coefficient rates derived from this study are available at <https://vesl.jpl.nasa.gov/solid-earth/gia>.

References

- Adhikari, S., Ivins, E. R., & Larour, E. (2016). ISSM-SESAW v1.0: Mesh-based computation of gravitationally consistent sea-level and geodetic signatures caused by cryosphere and climate driven mass change. *Geoscientific Model Development*, 9(3), 1087–1109. <https://doi.org/10.5194/gmd-9-1087-2016>
- Bevis, M., Wahr, J., Khan, S. A., Madsen, F. B., Brown, A., Willis, M., ... Francis, O. (2012). Bedrock displacements in Greenland manifest ice mass variations, climate cycles and climate change. *Proceedings of the National Academy of Sciences of the United States of America*, 109(30), 11,944–11,948.
- Blewitt, G., Kreemer, C., Hammond, W. C., & Gazeaux, J. (2016). MIDAS robust trend estimator for accurate GPS station velocities without step detection. *Journal of Geophysical Research: Solid Earth*, 121, 2054–2068. <https://doi.org/10.1002/2015JB012552>
- Bonin, J. A., Chambers, D. P., & Cheng, M. (2018). Using satellite laser ranging to measure ice mass change in Greenland and Antarctica. *The Cryosphere*, 12, 71–79. <https://doi.org/10.5194/tc-12-71-2018>
- Briggs, R. D., & Tarasov, L. (2013). How to evaluate model-derived deglaciation chronologies: A case study using Antarctica. *Quaternary Science Reviews*, 63, 109–127.
- Caron, L., Métyvier, L., Greff-Lefftz, M., Fleitout, L., & Rouby, H. (2017). Inverting glacial isostatic adjustment signal using Bayesian framework and two linearly relaxing rheologies. *Geophysical Journal International*, 209(2), 1126–1147.
- Cazenave, A., & Cozannet, G. L. (2014). Sea level rise and its coastal impacts. *Earth's Future*, 2, 15–34. <https://doi.org/10.1002/2013EF000188>
- Chambers, D. P., & Schröter, J. (2011). Measuring ocean mass variability from satellite gravimetry. *Journal of Geodynamics*, 52(5), 333–343.
- Chen, J., Wilson, C., Tapley, B., Save, H., & Cretaux, J.-F. (2017). Long-term and seasonal Caspian Sea level change from satellite gravity and altimeter measurements. *Journal of Geophysical Research: Solid Earth*, 122, 2274–2290. <https://doi.org/10.1002/2016JB013595>
- Chen, X., Zhang, X., Church, J. A., Watson, C. S., King, M. A., Monselesan, D., ... Harig, C. (2017). The increasing rate of global mean sea-level rise during 1993–2014. *Nature Climate Change*, 7(7), 492–495.
- Cheng, M., Ries, J. C., & Tapley, B. D. (2011). Variations of the Earth's figure axis from satellite laser ranging and GRACE. *Journal of Geophysical Research*, 116, B01409. <https://doi.org/10.1029/2010JB000850>
- Cronin, T. M., O'Regan, M., Pearce, C., Gemery, L., Toomey, M., Semiletov, I., & Jakobsson, M. (2017). Deglacial sea level history of the East Siberian Sea and Chukchi Sea margins. *Climate of the Past*, 13(9), 1097.
- Dyke, A., Andrews, J., Clark, P., England, J., Miller, G., Shaw, J., & Veillette, J. (2002). The Laurentide and Innuitian ice sheets during the Last Glacial Maximum. *Quaternary Science Reviews*, 21(1), 9–31.
- Eanes, R. J., & Bettadpur, S. V. (1996). Temporal variability of Earth's gravitational field from satellite laser ranging. In *Global gravity field and its temporal variations* (pp. 30–41). Berlin, Heidelberg: Springer.
- Eicker, A., Forootan, E., Springer, A., Longuevergne, L., & Kusche, J. (2016). Does GRACE see the terrestrial water cycle "intensifying"? *Journal of Geophysical Research: Atmospheres*, 121, 733–745. <https://doi.org/10.1002/2015JD023808>
- Famiglietti, J. S., & Rodell, M. (2013). Water in the balance. *Science*, 340(6138), 1300–1301.
- Flament, T., & Rémy, F. (2012). Dynamic thinning of Antarctic glaciers from along-track repeat radar altimetry. *Journal of Glaciology*, 58(211), 830–840.
- Gero, A., Wahr, J., & Zhong, S. (2013). Computations of the viscoelastic response of a 3-D compressible Earth to surface loading: An application to glacial isostatic adjustment in Antarctica and Canada. *Geophysical Journal International*, 192(2), 557–572.
- Gowan, E. J., Tregoning, P., Purcell, A., Montillet, J.-P., & McClusky, S. (2016). A model of the western Laurentide Ice Sheet, using observations of glacial isostatic adjustment. *Quaternary Science Reviews*, 139, 1–16.

- Hanebuth, T., Stattegger, K., & Bojanowski, A. (2009). Termination of the Last Glacial Maximum sea-level lowstand: The Sunda-Shelf data revisited. *Global and Planetary Change*, 66(1), 76–84.
- Holmes, S. A., & Featherstone, W. E. (2002). A unified approach to the Clenshaw summation and the recursive computation of very high degree and order normalised associated Legendre functions. *Journal of Geodesy*, 76(5), 279–299.
- Hsu, C.-W., & Velicogna, I. (2017). Detection of sea level fingerprints derived from GRACE gravity data. *Geophysical Research Letters*, 44, 8953–8961. <https://doi.org/10.1002/2017GL074070>
- Ivins, E. R., & James, T. S. (2004). Bedrock response to Llanquihue Holocene and present-day glaciation in southernmost South America. *Geophysical Research Letters*, 31, L24613. <https://doi.org/10.1029/2004GL021500>
- Ivins, E. R., James, T. S., Wahr, J., Schrama, O., Ernst, J., Landerer, F. W., & Simon, K. M. (2013). Antarctic contribution to sea level rise observed by GRACE with improved GIA correction. *Journal of Geophysical Research: Solid Earth*, 118, 3126–3141. <https://doi.org/10.1002/jgrb.50208>
- Ivins, E. R., Watkins, M. M., Yuan, D.-N., Dietrich, R., Casassa, G., & Rülke, A. (2011). On-land ice loss and glacial isostatic adjustment at the Drake Passage: 2003–2009. *Journal of Geophysical Research*, 116, B02403. <https://doi.org/10.1029/2010JB007607>
- Jekeli, C. (1981). Alternative methods to smooth the Earth's gravity field (Tech. Rep. 327). Columbus: Department of Geodesy Science Surveying, Ohio State University.
- Johnson, G. C., & Chambers, D. P. (2013). Ocean bottom pressure seasonal cycles and decadal trends from GRACE release-05: Ocean circulation implications. *Journal of Geophysical Research: Oceans*, 118, 4228–4240. <https://doi.org/10.1002/jgrc.20307>
- Jones, C. E., An, K., Blom, R. G., Kent, J. D., Ivins, E. R., & Bekaert, D. (2016). Anthropogenic and geologic influences on subsidence in the vicinity of New Orleans, Louisiana. *Journal of Geophysical Research: Solid Earth*, 121, 3867–3887. <https://doi.org/10.1002/2015JB012636>
- Karegar, M. A., Dixon, T. H., Malservisi, R., Kusche, J., & Engelhart, S. E. (2017). Nuisance flooding and relative sea-level rise: The importance of present-day land motion. *Scientific Reports*, 7(1), 11197.
- Kaufmann, G., Wu, P., & Ivins, E. R. (2005). Lateral viscosity variations beneath Antarctica and their implications on regional rebound motions and seismotectonics. *Journal of Geodynamics*, 39(2), 165–181. <https://doi.org/10.1016/j.jog.2004.08.009>
- Khan, S. A., Sasgen, I., Bevis, M., van Dam, T., Bamber, J. L., Wahr, J., . . . Munneke, P. K. (2016). Geodetic measurements reveal similarities between post-Last Glacial Maximum and present-day mass loss from the Greenland ice sheet. *Science Advances*, 2(9), e1600931. <https://doi.org/10.1126/sciadv.1600931>
- King, M. A., Bingham, R. J., Moore, P., Whitehouse, P. L., Bentley, M. J., & Milne, G. A. (2012). Lower satellite-gravimetry estimates of Antarctic sea-level contribution. *Nature*, 491(7425), 586–589.
- Kuchar, J., Milne, G., Wolstencroft, M., Love, R., Tarasov, L., & Hijma, M. (2017). The influence of sediment isostatic adjustment on sea-level change and land motion along the US Gulf coast. *Journal of Geophysical Research: Solid Earth*, 122. <https://doi.org/10.1002/2017JB014695>
- Lambeck, K., Purcell, A., Johnston, P., Nakada, M., & Yokoyama, Y. (2003). Water-load definition in the glacio-hydro-isostatic sea-level equation. *Quaternary Science Reviews*, 22(2), 309–318.
- Lambeck, K., Purcell, A., & Zhao, S. (2017). The North American Late Wisconsin ice sheet and mantle viscosity from glacial rebound analyses. *Quaternary Science Reviews*, 158, 172–210.
- Lambeck, K., Purcell, A., Zhao, J., & Svenson, N.-O. (2010). The Scandinavian ice sheet: From MIS 4 to the end of the Last Glacial Maximum. *Boreas*, 39(2), 410–435.
- Lambeck, K., Rouby, H., Purcell, A., Sun, Y., & Sambridge, M. (2014). Sea level and global ice volumes from the Last Glacial Maximum to the Holocene. *Proceedings of the National Academy of Sciences of the United States of America*, 111(43), 15,296–15,303.
- Llovel, W., Willis, J., Landerer, F., & Fukumori, I. (2014). Deep-ocean contribution to sea level and energy budget not detectable over the past decade. *Nature Climate Change*, 4(11), 1031–1035.
- Martin-Español, A., Zammit-Mangion, A., Clarke, P. J., Flament, T., Helm, V., King, M. A., . . . Bamber, J. L. (2016). Spatial and temporal Antarctic ice sheet mass trends, glacio-isostatic adjustment, and surface processes from a joint inversion of satellite altimeter, gravity, and GPS data. *Journal of Geophysical Research: Earth Surface*, 121, 182–200. <https://doi.org/10.1002/2015JF003550>
- Martinec, Z., Sasgen, I., & Velimský, J. (2014). The forward sensitivity and adjoint-state methods of glacial isostatic adjustment. *Geophysical Journal International*, 200(1), 77–105.
- McMillan, M., Shepherd, A., Sundal, A., Briggs, K., Muir, A., Ridout, A., . . . Wingham, D. (2014). Increased ice losses from Antarctica detected by CRYOSAT-2. *Geophysical Research Letters*, 41, 3899–3905. <https://doi.org/10.1002/2014GL060111>
- Milne, G. A., Davis, J. L., Mitrovica, J. X., Scherneck, H.-G., Johansson, J. M., Vermeer, M., & Koivula, H. (2001). Space-geodetic constraints on glacial isostatic adjustment in Fennoscandia. *Science*, 291(5512), 2381–2385.
- Milne, G. A., Long, A. J., & Bassett, S. E. (2005). Modelling Holocene relative sea-level observations from the Caribbean and South America. *Quaternary Science Reviews*, 24(10), 1183–1202.
- Milne, G. A., & Mitrovica, J. X. (1998). Postglacial sea-level change on a rotating Earth. *Geophysical Journal International*, 133(1), 1–19.
- Mitrovica, J. X., Hay, C. C., Morrow, E., Kopp, R. E., Dumberry, M., & Stanley, S. (2015). Reconciling past changes in Earth's rotation with 20th century global sea-level rise: Resolving Munk's enigma. *Science Advances*, 1(11), e1500679.
- Morison, J., Wahr, J., Kwok, R., & Peralta-Ferriz, C. (2007). Recent trends in Arctic ocean mass distribution revealed by GRACE. *Geophysical Research Letters*, 34, L07602. <https://doi.org/10.1029/2006GL029016>
- Murray-Wallace, C. V., & Woodroffe, C. D. (2014). *Quaternary sea-level changes: A global perspective*. Cambridge, UK: Cambridge University Press. <https://doi.org/10.1017/CBO9781139024440>
- Nilsson, J., Gardner, A., Sandberg, L., Sørensen, & Forsberg, R. (2016). Improved retrieval of land ice topography from CryoSat-2 data and its impact for volume-change estimation of the Greenland ice sheet. *The Cryosphere*, 10(6), 2953–2969.
- Nordman, M., Milne, G., & Tarasov, L. (2015). Reappraisal of the Ångerman River decay time estimate and its application to determine uncertainty in Earth viscosity structure. *Geophysical Journal International*, 201(2), 811–822.
- Paulson, A., Zhong, S., & Wahr, J. (2007). Inference of mantle viscosity from GRACE and relative sea level data. *Geophysical Journal International*, 171(2), 497–508.
- Peltier, W. (2004). Global glacial isostasy and the surface of the ice-age Earth: The ICE-5G (VM2) model and GRACE. *Annual Review of Earth and Planetary Sciences*, 32, 111–149.
- Peltier, W., Argus, D., & Drummond, R. (2015). Space geodesy constrains ice age terminal deglaciation: The global ICE6G_C (VM5a) model. *Journal of Geophysical Research: Solid Earth*, 120, 450–487. <https://doi.org/10.1002/2014JB011176>
- Ponte, R. M., & Piecuch, C. G. (2014). Interannual bottom pressure signals in the Australian–Antarctic and Bellingshausen Basins. *Journal of Physical Oceanography*, 44(5), 1456–1465.
- Purcell, A., Tregoning, P., & Dehecq, A. (2016). An assessment of the ICE6G_C (VM5a) glacial isostatic adjustment model. *Journal of Geophysical Research: Solid Earth*, 121, 3939–3950. <https://doi.org/10.1002/2015JB012742>
- Quinn, K. J., & Ponte, R. M. (2010). Uncertainty in ocean mass trends from GRACE. *Geophysical Journal International*, 181(2), 762–768.

- Reager, J., Gardner, A., Famiglietti, J., Wiese, D., Eicker, A., & Lo, M.-H. (2016). A decade of sea level rise slowed by climate-driven hydrology. *Science*, 351(6274), 699–703.
- Richter, A., Ivins, E., Lange, H., Mendoza, L., Schroder, L., Hormaechea, J., ... Dietrich, R. (2016). Crustal deformation across the Southern Patagonian icefield observed by GNSS. *Earth and Planetary Science Letters*, 452, 206–215.
- Rietbroek, R., Brunnabend, S.-E., Kusche, J., Schröter, J., & Dahle, C. (2016). Revisiting the contemporary sea-level budget on global and regional scales. *Proceedings of the National Academy of Sciences of the United States of America*, 113(6), 1504–1509.
- Roy, K., & Peltier, W. (2017). Space-geodetic and water level gauge constraints on continental uplift and tilting over North America: Regional convergence of the ICE-6G_C (VM5a/VM6) models. *Geophysical Journal International*, 210(2), 1115–1142.
- Sasgen, I., Klemann, V., & Martinec, Z. (2012). Towards the inversion of GRACE gravity fields for present-day ice-mass changes and glacial-isostatic adjustment in North America and Greenland. *Journal of Geodynamics*, 59, 49–63.
- Sasgen, I., Martín-Español, A., Horvath, A., Klemann, V., Petrie, E. J., Wouters, B., ... Drinkwater, M. R. (2017). Joint inversion estimate of regional glacial isostatic adjustment in Antarctica considering a lateral varying Earth structure (ESA STSE project REGINA). *Geophysical Journal International*, 211(3), 1534–1553. <https://doi.org/10.1093/gji/ggx368>
- Save, H., Bettadpur, S., & Tapley, B. D. (2012). Reducing errors in the GRACE gravity solutions using regularization. *Journal of Geodesy*, 86(9), 695–711.
- Save, H., Bettadpur, S., & Tapley, B. D. (2016). High-resolution CSR GRACE RL05 mascons. *Journal of Geophysical Research: Solid Earth*, 121, 7547–7569. <https://doi.org/10.1002/2016JB013007>
- Schumacher, M., Kusche, J., & Döll, P. (2016). A systematic impact assessment of GRACE error correlation on data assimilation in hydrological models. *Journal of Geodesy*, 90(6), 537–559.
- Sella, G. F., Stein, S., Dixon, T. H., Craymer, M., James, T. S., Mazzotti, S., & Dokka, R. K. (2007). Observation of glacial isostatic adjustment in “stable” North America with GPS. *Geophysical Research Letters*, 34, L02306. <https://doi.org/10.1029/2006GL027081>
- Shepherd, A., Ivins, E. R., Geruo, A., Barletta, V. R., Bentley, M. J., Bettadpur, S., ... Jay Zwally, H. (2012). A reconciled estimate of ice-sheet mass balance. *Science*, 338(6111), 11,83–11,89.
- Simon, K., Riva, R., Kleinherenbrink, M., & Tangdamrongsub, N. (2017). A data-driven model for constraint of present-day glacial isostatic adjustment in North America. *Earth and Planetary Science Letters*, 474, 322–333.
- Sošnica, K., Jäggi, A., Meyer, U., Thaller, D., Beutler, G., Arnold, D., & Dach, R. (2015). Time variable Earth's gravity field from SLR satellites. *Journal of Geodesy*, 89(10), 945–960.
- Swenson, S., & Wahr, J. (2006). Post-processing removal of correlated errors in GRACE data. *Geophysical Research Letters*, 33, L08402. <https://doi.org/10.1029/2005GL025285>
- Tamisiea, M., Mitrovica, J., & Davis, J. (2007). GRACE gravity data constrain ancient ice geometries and continental dynamics over Laurentia. *Science*, 316(5826), 881–883.
- Tamisiea, M. E. (2011). Ongoing glacial isostatic contributions to observations of sea level change. *Geophysical Journal International*, 186(3), 1036–1044.
- Tarasov, L., Dyke, A. S., Neal, R. M., & Peltier, W. (2012). A data-calibrated distribution of deglacial chronologies for the North American ice complex from glaciological modeling. *Earth and Planetary Science Letters*, 315-316(Supplement C), 30–40. <https://doi.org/10.1016/j.epsl.2011.09.010>
- van der Wal, W., Whitehouse, P. L., & Schrama, E. J. (2015). Effect of GIA models with 3D composite mantle viscosity on grace mass balance estimates for Antarctica. *Earth and Planetary Science Letters*, 414, 134–143. <https://doi.org/10.1016/j.epsl.2015.01.001>
- Velicogna, I., & Wahr, J. (2013). Time-variable gravity observations of ice sheet mass balance: Precision and limitations of the GRACE satellite data. *Geophysical Research Letters*, 40, 3055–3063. <https://doi.org/10.1002/grl.50527>
- Verleyen, E., Tavernier, I., Hodgson, D. A., Whitehouse, P. L., Kudoh, S., Imura, S., ... Vyvermana, W. (2017). Ice sheet retreat and glacio-isostatic adjustment in Lützow-Holm Bay, East Antarctica. *Quaternary Science Reviews*, 169, 85–98.
- Vermeersen, L., Sabadini, R., & Spada, G. (1996). Compressible rotational deformation. *Geophysical Journal International*, 126(3), 735–761.
- Wahr, J., Molenaar, M., & Bryan, F. (1998). Time variability of the Earth's gravity field: Hydrological and oceanic effects and their possible detection using GRACE. *Journal of Geophysical Research*, 103(B12), 30,205–30,229.
- Watkins, M. M., Wiese, D. N., Yuan, D.-N., Boening, C., & Landerer, F. W. (2015). Improved methods for observing Earth's time variable mass distribution with GRACE using spherical cap mascons. *Journal of Geophysical Research: Solid Earth*, 120, 2648–2671. <https://doi.org/10.1002/2014JB011547>
- Whitehouse, P. L., Bentley, M. J., & Le Brocq, A. M. (2012). A deglacial model for Antarctica: Geological constraints and glaciological modelling as a basis for a new model of Antarctic glacial isostatic adjustment. *Quaternary Science Reviews*, 32, 1–24.
- Whitehouse, P. L., Bentley, M. J., Milne, G. A., King, M. A., & Thomas, I. D. (2012). A new glacial isostatic adjustment model for Antarctica: Calibrated and tested using observations of relative sea-level change and present-day uplift rates. *Geophysical Journal International*, 190(3), 1464–1482.
- Wieczorek, M. A., Meschede, M., Oshchepkov, I., Sales de Andrade, E., & heroxbd (2016). SHTOOLS: Version 4.0. <https://doi.org/10.5281/zenodo.206114>
- Wiese, D. N., Landerer, F. W., & Watkins, M. M. (2016). Quantifying and reducing leakage errors in the JPL RL05M GRACE mascon solution. *Water Resources Research*, 52, 7490–7502. <https://doi.org/10.1002/2016WR019344>
- Wouters, B., Bonin, J. A., Chambers, D. P., Riva, R. E. M., Sasgen, I., & Wahr, J. (2014). GRACE, time-varying gravity, Earth system dynamics and climate change. *Reports on Progress in Physics*, 77(11), 116801.
- Wu, X., Heflin, M. B., Schotman, H., Vermeersen, B. L., Dong, D., Gross, R. S., ... Owen, S. E. (2010). Simultaneous estimation of global present-day water transport and glacial isostatic adjustment. *Nature Geoscience*, 3(9), 642–646.